# Upper-bound General Circulation of Coupled Ocean-Atmosphere:

# Part 2. Ocean

Hsien-Wang Ou[1]

Lamont-Doherty Earth Observatory, Columbia University

Palisades, NY 10964 (Retired)

3/2/2021

[1]Author: Hsien-Wang Ou, hsienou0905@gmail.com

## Key Points:

- We deduce the general ocean circulation (GOC) within the thermodynamic closure of a coupled ocean-atmosphere system.
- We assume the potential vorticity to be homogenized in the warm layer above the main thermocline to derive the upper-bound GOC.
- The model GOC resembles the observed one, suggesting that the latter may be explained by the PV mixing in place of the Sverdrup dynamics.


## Abstract

This two-part paper considers the general circulation of the atmosphere (Part 1) and ocean (Part 2) within the deductive framework of our climate theory, which aims to derive the earth's generic climate state from first principles. Because the planetary fluids are inherently turbulent, such state is a macroscopic manifestation of a nonequilibrium thermodynamic system, whose closure involves the maximum entropy production, a veritable generalization of the second fundamental law. The logical progression detailed in the preceding papers of the theory has reduced the planetary fluids to warm and cold thermal masses and determined their bulk properties, which provide the prior constraints for the present dynamical derivation. Consistent with the asymptotic thermal state, we assume the potential vorticity (PV) to be homogenized in thermal masses to derive the upper-bound general circulations. In Part 1, this upper bound is seen to resemble the prevailing wind, forsaking therefore discordant explanations of the easterly trades and the polar jet stream. In this Part 2, we show again that this upper-bound may reproduce the observed general ocean circulation, suggesting that the latter may be explained by PV mixing ---

in place of the laminar Sverdrup dynamics. Together with Part 1, we posit that the general planetary circulations are the maximum flow extractable by random eddy mixing when subjected to differential solar heating.

## Plain Language Summary

Given teeming eddies observed in the ocean and their demonstrated efficacy in mixing conservative properties, we consider an asymptotic state of the ocean when the temperature and potential vorticity are homogenized in the warm watermass. The resulting upper-bound circulation broadly resembles the observed one, suggesting that the general ocean circulation may be interpreted as the maximum flow extractable by random eddy mixing within the confine of the thermal differentiation.

### 1. Introduction

With the advent of the satellite imaging, teeming eddies have emerged as a defining character of the ocean motion field (Fu et al., 2010), but despite the seemingly random (microscopic) motion, the time-averaged (macroscopic) flow exhibits nonetheless persistent large-scale structure, which defines the general ocean circulation (GOC, all acronyms are listed in Appendix A) of our inquiry. To limit our scope however, we are concerned only with the vertical-averaged flow above the main thermocline in an ocean confined between meridional boundaries, excluding therefore the circumpolar current, the deep circulation, as well as the shallow tropical circulation.

One of the most prominent features of the GOC is the western-intensified subtropical gyre, whose explanation by Stommel (1948) arguably heralded the modern wind-driven theories.

For simplicity, Stommel considers a homogeneous ocean whereby the wind curl would propel a meridional flow of the same sign (that is, equatorward for an anticyclonic wind) via the Sverdrup (1947) balance and since the gyre is also of this sign --- to provide the requisite frictional sink, it is *de facto* western-intensified. Since the observed gyre is largely limited to above the main thermocline, Welander (1968) has applied the Sverdrup balance to the upper-layer flow, which retains the western intensification although key thermal properties need to be prescribed. Luyten et al. (1983) have appended additional shallow immiscible layers (the ventilated thermocline) to produce intricate circulation of the subducted water, but since the main thermocline is defined by the reach of the vertical mixing (Colin de Verdière, 1989; Salmon, 1990; Samelson & Vallis, 1997), such immiscibility needs justification. In any event, the ventilated thermocline has little impact on the subtropical gyre, which is largely unsheltered from the surface wind. More seriously however, the model gyre is bounded to the north by the maximum westerly where the Sverdrup flow vanishes, whereas observationally the gyre boundary is marked by a prominent subtropical front --- the outcrop of the main thermocline (McCartney, 1982).

Such outcrop would emerge if the thermocline along the eastern boundary is sufficiently shallow, a depth that is not constrained by physical balances but assigned from observation (Parsons, 1969; Veronis, 1973; Huang & Flierl, 1987). And then the arched appearance of the outcrop, which would extend to the northern limit of the basin, contrasts sharply the generally zonal orientation of a mid-latitude subtropical front --- reflecting its control by the differential solar heating. Clearly, the subtropical gyre can be explained only in conjunction with the heat balance that constrains this thermal boundary.

The coupling of the heat balance and the GOC has been investigated by numerical models, for which the ocean temperature is often restored to a hypothetical air temperature, a proxy of the differential solar heating (Haney, 1971). Such numerical models have shown ever apparent need to resolve eddies, as expounded next. For coarse-grid calculations that do not resolve eddies, the differential heating is countered by a laminar meridional overturning circulation (MOC), whose strength depends strongly on the diapycnal diffusivity, a highly uncertain property of the ocean. For a small diapycnal diffusivity hence weak MOC, the ocean temperature would approach the restoring temperature, thus containing no front (Cox, 1985). The diffused temperature thus plays only a passive role to the gyre boundary, which remains aligned with the maximum westerly; such weak MOC and subtropical front obviously do not comport with observations. Employing a greater diapycnal diffusivity to replicate the observed strength of the MOC on the other hand would push the warm water toward the northern wall of the basin accompanied by a broad eastward flow (Colin de Verdière, 1989), differing again from the observed situation.

This difficulty in reconciling the MOC strength and the mid-latitude positioning of the front can be alleviated by fine-grid calculations that resolve eddies. Since eddies can transport heat (Greatbatch et al., 2007), they lessen the need of a strong throughflow and the attendant advection of the warm water, thus allowing a mid-latitude front; and then the eddies, by mixing the warm water, would sharpen in effect the subtropical front. Being regulated by eddy mixing, the front need not be aligned with the maximum westerly (Liu et al., 2021, personal communication) and, more strikingly still, it remains at mid-latitudes even when the wind is shut off (Hogg & Gayen, 2020). No explanations however are given as to how the eddy dynamics sets the latitude of the subtropical front, a question to be addressed later.

Besides mixing the temperature of the warm watermass, eddies also mix the potential vorticity (PV), the dynamical counterpart to the temperature because of their similar material conservation. While mixing of the PV is well discerned in numerical models and observations (Holland et al., 1984), less recognized however is that the differential wind is in fact weaker than the differential heating in relative terms, so the PV would mix more thoroughly than the temperature (Section 4), as indeed the observed case. And since the two-layer ocean has been widely applied in wind-driven theories --- justifiable by visual inspection of the hydrographic data, it is only physically consistent that the PV be assumed uniform as well in the warm layer. While one may hash over the efficacy of PV mixing, we are nonetheless justified to examine the asymptotic state of homogenized PV and its attendant upper-bound GOC, and if this upper bound bears resemblance to the observed GOC, the PV mixing may provide a plausible explanation.

Besides the central role played by eddies, our theory of the GOC also differs from the previous ones in that it is couched within the thermodynamic closure of a coupled ocean-atmosphere system. The formulation of such closure has been an ongoing effort of this author with the aim of deriving the generic climate state from first principles. The previous steps contained in a series of papers (Ou, 2001, 2006, 2007) have reduced the planetary fluids to warm and cold thermal masses and determine their bulk properties, and since the derivation involves only thermodynamics, they can be regarded as known for the dynamical derivation contained in this two-part paper.

Consistent with the asymptotic thermal state, we posit that the PV is homogenized in active thermal masses to derive the upper-bound general circulation. In Part 1 on the general at-

mospheric circulation (GAC, Ou, 2013), we show that this upper-bound may replicate the prevailing wind, forsaking therefore discordant explanations of the easterly trades and the polar jet stream. In this Part 2 on the GOC, we shall show again that this upper bound may reproduce broadly the observed GOC, suggesting that the latter may be explained by the PV homogenization in an eddying ocean --- in place of the laminar Sverdrup dynamics.

For the organization of this Part 2, we first recount in Section 2 the logical progression leading to a two-layer ocean and certain bulk properties of the outcropped thermocline. In Section 3, we consider the mechanical energy (ME) balance in constraining the mean thermocline depth hence the homogenized PV. In Section 4, we assess the PV homogenization and its computational and observational evidence. Subjected to prior constraints, we proceed in Section 5 to derive the upper-bound GOC and compare it with the observed one. In Section 6, we provide a critique of the Sverdrup dynamics via its contrast with the homogenized PV. In Section 7, we summarize the main findings of this paper, which concludes our climate theory.

## 2. Prior Constraints

To assure the deductibility of our GOC, we shall first recount the logical progression of our climate theory in setting the prior thermal constraints. Since the planetary fluids are inherently turbulent, the central tenet of our theory is that the climate state is a macroscopic manifestation of a nonequilibrium thermodynamic (NT) system hence subjected to the maximum entropy production (MEP) --- a verifiable generalization of the second fundamental law (Kleidon, 2009; Ozawa et al., 2003). Employing the MEP, we first determine the global-mean surface temperature given the solar insolation (Ou, 2001), which provides a constraint on the meridional thermal

field (Ou, 2006). For the latter, we first invoke laboratory experiments on the horizontal convection (Rossby, 1965) and eddy mixing of the buoyant layer to divide the ocean into warm and cold thermal masses separated by an outcropped thermocline, a well-discerned first-order description of the observed ocean. We then apply the MEP to the troposphere to reduce it to two thermal masses as well with their surface temperature linked to that of the surface ocean. Again, the two thermal masses correspond to the observed tropical and polar airmasses separated by the polar front.

As an asymptotic state of the ocean, we therefore consider a thermal configuration as sketched in Fig. 1, which consists of a moving warm layer separated from the motionless cold water by an outcropped thermocline. The ocean is heated differentially by the absorbed solar flux $q$ (symbols and standard values are listed in Appendix B) and forced by the wind stress $\tau^*$, and the prior constraints to be derived below are the outcrop latitude ($l$), the reduced gravity ($g'$) and the mean depth ($\bar{h}$) of the thermocline as well as the mass-exchange rate ($K$) associated with the MOC. For obvious reasons, we can only provide abbreviated derivations and readers can consult cited papers for more detailed discussion.

The differential heat balance (that is, removing the global means) is of the form,

$$\rho_o C_{p,o} K(T_1 - T_2) = \int_0^l (q - \alpha T_1/2) dy, \quad (1)$$

which states that the absorbed solar flux minus the convective cooling of the warm layer (the right-hand-side or rhs) is balanced on the left-hand-side (lhs) by the heat flux across the subtropical front, the latter being a product of the mass exchange rate and the differential temperature. Noting that we have already incorporated the thermal coupling of the atmosphere, as reflected in

the ½ factor in the convective cooling (Ou, 2006). The MOC is a generalization of the laminar overturning cell to include random eddy shedding, the latter in fact dominates the throughflow based on eddy census (Auer, 1987). There is however no need to discern the partition of the two: so long as the eddy shedding is nonzero, the MOC is subjected to microscopic fluctuations hence the MEP (Ou, 2018).

For simplicity, we assume that the absorbed solar flux decreases linearly with the latitudinal distance *y* with a total range $\Delta q$ and scale the differential temperature by $[T] = \alpha^{-1}\Delta q$ (brackets for scales), the distance by $[y] = L$ (the hemispheric basin length), and the MOC by $[K] = \gamma L$ where $\gamma \equiv \left(\rho_o C_{p,0}\right)^{-1}\alpha$ is referred as the air-sea exchange velocity. Applying these scales, the heat balance Eq. (1) is nondimensionalized (hence primed) to

$$K'\Delta T' = \int_0^{l'} \left(\frac{1}{2} - y - \frac{1}{2}T_1'\right) dy, \tag{2}$$

where $\Delta T' = T_1' - T_2'$ is the differential temperature. Subject to the net balance of

$$l'T_1' + (1 - l')T_2' = 0, \tag{3}$$

Eq. (2) can be expressed in the differential temperature as

$$K'\Delta T' = \frac{1}{2}\, l'(1 - l')(1 - \Delta T'). \tag{4}$$

The entropy production $\sigma$ is the product of the thermodynamic force ($\Delta T'$) and flux ($K'\Delta T'$) hence,

$$\sigma = K'\Delta T'\Delta T'$$

$$= \frac{1}{2}\, l'(1-l')(1-\Delta T')\Delta T'. \tag{5}$$

Maximizing Eq. (5) with respect to $l'$ and $\Delta T'$ individually yields

$$l' = \Delta T' = 1/2, \tag{6}$$

so the MOC is

$$K' = 1/8. \tag{7}$$

It is seen that the MEP yields surprisingly simple expressions for these thermal properties, but how do they compare with models or observations? The mid-latitude position of the front has been demonstrated by numerical calculations when the wind is shut off (Hogg & Gayen, 2020) and it is consistent with its observed commonality in all ocean basins and both hemispheres. It can be readily explained by the MEP: if the front were to displace from the mid-latitude, Eq. (5) implies a weaker heat flux hence entropy production, in contradiction to the MEP. For a basin length of $L$ = 8000 km, we have then $l$ = 4000 km or the warm layer extends to about $40^0$N, not unlike that observed. The differential temperature has a dimensional expression $\Delta T = (2\alpha)^{-1}\Delta q$, so if one takes $\Delta q = 300\ W\ m^{-2}$, $\alpha = 15\ W\ m^{-2}\ {}^0\mathrm{C}^{-1}$ (Ou, 2018), this differential temperature is 10 $^0$C, just as observed (Bower & Hogg, 1996). The MOC has a dimensional flux of $K = \gamma L/8$ and, applying standard values, the air-sea exchange velocity is $\gamma = 3.6 \times 10^{-6}\ m\ s^{-1}$, so $K = 3.6\ m^2\ s^{-1}$. For a basin width of 6000 km, it yields a MOC transport of 21.6 Sv, which is commensurate with its observed value (Macdonald, 1998).

A laminar MOC would depend on both the density stratification and the diapycnal diffusivity (Colin de Verdière, 1988), the latter in particular is a highly uncertain property of the

ocean, which in fact is finely tuned in numerical models to produce the required MOC (Rahmstorf et al., 2005). In contrast, in an eddying ocean, the MOC is independent of both these properties and, even more surprisingly, the absorbed solar flux --- the ultimate source of the ocean heating. The reason for this robustness is because the ocean temperature would adjust in tandem with the radiative heating to insulate its effect on the MOC. The heat transport carried by the MOC does however vary with the differential solar heating, which moreover can be regulated by the large-scale wind (Lozier, 2010) via the air-sea exchange coefficient.

The above MEP solution implies that the atmospheric heat transport equals the oceanic one hence is known (Ou, 2006). Subjected to the Clausius–Clapeyron scaling, Ou (2007) then deduces the poleward moisture transport whose return in the ocean then specifies the differential salinity and, together with the differential temperature, the reduced gravity. With the density contrast and the MOC known, Ou (2007) surmises that the ME balance would constrain the thermocline depth, but he did not carry out the derivation, which is now provided below.

## 3. Thermocline depth

The mechanical energy balance of the ocean is of the form (Huang, 1999; Hughes et al., 2009)

$$\tfrac{1}{2}K\bar{h}g' = \nu l g' + \int_0^l \tau u dy, \tag{8}$$

where $\nu$ is the vertical diffusivity in the warm layer, $\tau = \tau^*/\varrho_o$, the zonal wind stress per unit water density and $u$, the zonal current. The rhs represents the ME source due to the vertical mixing and the wind work, respectively, both assumed dominated by the warm layer, and the lhs is the expenditure of the ME by the MOC. Although the differential heating imparts no potential

energy to the ocean, it does generate available potential energy (APE, Hughes et al., 2009), which feeds the eddies via the baroclinic instability (Holland & Lin, 1975). It is the conversion of the eddy kinetic energy, together with other external sources, such as tides and geothermal flux, that cause the vertical mixing. Since we remain uncertain about energy pathways and scalings (Huang, 1999; Ferrari & Wunsch, 2009; Vreugdenhil et al., 2016), we shall simply assign a plausible vertical diffusivity in later calculations, an acknowledged gap in our closure.

Since the wind work involves the zonal current --- an internal property, it needs further examination to isolate the external forcing. For this, we first note that the wind work is dominated by that acting on the frontal jet since although the easterly trade is substantial, its work is somewhat nullified by the alternating tropical currents (Wunsch, 1998). And then the narrowness and geostrophic balance of the frontal jet lead to the following relation

$$\int_0^l \tau u dy \approx -g' \frac{\tau_1}{f_1} \int_0^l h_y dy \tag{9}$$

$$= g' \bar{h} K_E, \tag{10}$$

where subscripts "1" indicate the values at the outcrop and

$$K_E = \tau_1 / f_1 \tag{11}$$

is the "Ekman" transport crossing the outcrop. Substituting Eq. (10) into Eq. (8), we derive

$$\bar{h} = h_m (1 - 2K_E/K)^{-1}, \tag{12}$$

where

$$h_m = 2\nu l/K \tag{13}$$

is the thermocline depth due to the vertical mixing alone, which we shall refer as the "mixed" layer depth. It is seen that the mean thermocline depth is now specified by the prior constraints (including the maximum westerly determined in Part 1). For an estimate, we use $\nu = 10^{-4}\ m^2\ s^{-1}$ (Colin de Verdière, 1989) and standard parameter values to yield $h_m = 220\ m$. Setting additionally $\tau_1 = 10^{-4} m^2\ s^{-2}$ (a wind stress of .1 $N\ m^{-2}$) and $f_1 = .9 \times 10^{-4} s^{-1}$, the mean thermocline depth would be $\bar{h} = 575\ m$, not unlike that observed (McCartney, 1982, his Fig. 3, taking $\sigma_t$ = 27 as the thermocline). Given its sensitive dependence on external parameters, the above exercise serves only to demonstrate that the MEP solution with plausible external parameters can produce the observed thermocline depth. As a further test, the standard parameter values yield a mean wind-work of $2.75 \times 10^{-3} W\ m^{-2}$ over the warm layer, which is of the same order of its previous estimate (Wunsch, 1998, his Table 1).

From Eq. (12), we see that a stronger vertical mixing or wind work would deepen the thermocline whereas a stronger MOC hence the loss of the ME would have the opposite effect. Less expected however is the growing importance of the wind as it enters through the denominator of the expression. We can trace this to the positive feedback between the wind work and the frontal jet: increasing the wind work would deepen the thermocline to strengthen the zonal current, which in turn augments the wind work.

## 4. PV homogenization

We have considered the asymptotic state of infinite eddy diffusivity in the warm layer, and since the microscopic PV is materially conserved, its macroscopic representation would be

homogenized in the warm layer as well. We shall next assess this approximation when the eddy diffusivity $k$ is finite, in which case the macroscopic PV is subjected to the balance (Young, 1987, his Eqs. [3.5], [4.2] and [4.3])

$$\vec{v} \cdot \nabla P - \nabla \cdot (k \nabla P) = h^{-1} \hat{k} \cdot \nabla \times (\vec{\tau}/h), \tag{14}$$

where

$$P \equiv h^{-1}(f + \hat{k} \cdot \nabla \times \vec{v}) \tag{15}$$

is the columnar PV. This equation states that the wind curl is countered by the mean advection and eddy mixing of the PV. In the laminar regime ($k$ = 0) and neglecting the relative vorticity, Eq. (14) would reduce to the familiar Sverdrup balance (generalized to the moving upper layer)

$$\beta h v_s = \hat{k} \cdot \nabla \times \vec{\tau}, \tag{16}$$

where $\beta$ is the gradient of the Coriolis parameter and $v_s$, the Sverdrup flow; but with increasing eddy diffusivity, the PV should approach a harmonic function.

Nondimensionalizing the PV by its unmixed range $\Delta P = \beta l/\bar{h}$, it has a Laplacian of the order ("~")

$$\nabla^2 P' \sim \varepsilon_P = t_m/t_s, \tag{17}$$

where

$$t_m = l^2/k \tag{18}$$

is the basin "mixing" time and

$$t_s = l/v_s \tag{19}$$

is the "Sverdrup" time that it takes for the Sverdrup flow to traverse the warm layer. Based on observations, we take $k = 5 \times 10^4\ m^2\ s^{-1}$ (LaCasce & Bower, 2000; Ollitrault et al., 2005) and $l = 4 \times 10^3$ km to yield $t_m \sim 10\ y$. We note that the eddy diffusivity is a proxy of the microscopic stirring, which is particularly effective by the chaotic advection (Brown & Smith, 1991). The latter in fact would homogenize the PV at the basin-scale first before smoothing it at smaller (still macroscopic) scale, so the eddy diffusivity is a global property that cannot be deduced from turbulence closure or diagnosed from local measurement, such as Krauss & Böning (1987). For this reason, the basin mixing time provides a better measure of the PV homogenization (Pierrehumbert, 1991), and its estimated decadal duration is supported by other independent analyses, including the following: 1) eddy-resolving calculations show that the two-particle correlation function has stabilized down to the deformation radius in about a decade (Berloff et al., 2002, their Fig. 17); 2) such calculations also show that numerical particles released at a point spread through the gyre in about a decade (Nakamura & Kagimoto, 2006); 3) tritium-$^3$He age distributions show a basin-wide ventilation time of about a decade (Jenkins, 1988); 4) satellite censuses show eddy migration of several kilometers a day (Chelton et al., 2007), which would traverse the basin in a decade.

To estimate the Sverdrup time, we set $\Delta\tau = 10^{-4} m^2 \cdot s^{-2}$, $h$ = .5 km and $\beta = 2 \times 10^{-11} m^{-1}\ s^{-1}$ in Eq. (16) to yield $v_s \sim 2.5 \times 10^{-3} m\ s^{-1}$ hence $t_s \sim 50\ y$. As this time is several times the eddy mixing time or $\varepsilon_P \sim .2$, the PV should approach a harmonic function. Since the PV flux is finite across the lateral boundary to flush out the net wind-curl (Harrison, 1981),

301 the normal PV gradient should vanish as well in the asymptotic limit. Subjected to this Neu-
302 mann condition, the harmonic PV would be a constant or the PV is homogenized (Hilderbrand,
303 1962).

304 Physically, the strong eddy mixing would expel the PV gradient to the boundary, thus ho-
305 mogenizing the PV in the interior. Noting that this boundary includes the equator since a ho-
306 mogenized hence finite PV necessarily implies an equatorial front because of its hemispheric
307 symmetry, a situation that differs qualitatively from that of the troposphere whereby the seasonal
308 migration of the ITCZ amounts to strong cross-equatorial mixing to yield a zero tropical PV.
309 The deduction of an oceanic front at the equator naturally resolves a significant difficulty en-
310 countered by Salmon (1982) and it is consistent with the observed tracer barrier there (Fine et al.,
311 1987). Our deduction of a homogenized PV by strong eddy mixing should be distinguished from
312 that based on the Prandtl–Batchelor theorem (Rhines & Young, 1982), which is predicated on
313 weak eddy mixing; such weak mixing is required for the PV to be conserved hence constant
314 along a closed streamline, which then diffuses inward to homogenize the PV. It should be
315 stressed that in an eddying ocean, only the microscopic PV is conserved, as seen in its filamen-
316 tary appearance (Turiel et al., 2009), and it is precisely this conservation that causes the homoge-
317 nization on the macroscopic scale. Then even in the weak mixing regime, the conservation of a
318 macroscopic PV on a streamline could be thwarted by the wind curl or when the streamline
319 transits through the frictional boundary layer (Ierley & Young, 1983).

320 It is instructive to assess relative homogenization of the PV with respect to that of the
321 temperature. The Laplacian of the warm-layer temperature corresponding to Eq. (17) is

322 $$\nabla^2 T' \sim \varepsilon_T = t_m / t_r, \tag{20}$$

where the restoring timescale $t_r$ can be seen from Eq. (1) to be

$$t_r = \bar{h}/\gamma. \tag{21}$$

Applying the standard parameter values, we estimate $t_r \sim 5\ y$. Since it is of the same order as the eddy mixing time, we do not expect strong mixing of the warm-layer temperature even though the two-layer approximation may remain applicable by the sharpness of the subtropical front. The ratio of the PV to the temperature range is given by $\varepsilon_P/\varepsilon_T = t_r/t_s \sim .1$, which measures the relative strength of the differential wind forcing versus the differential solar heating. Because of the smallness of this ratio, the PV should homogenize to a greater degree than the temperature, as indeed the observed case; and if one were to adopt the two-layer approximation, the physical consistency seems to demand that the PV be assumed uniform in the warm layer as well.

For computational supports, eddy-resolving numerical calculations have shown discernible homogenization of the upper-ocean PV in the subtropics even when it is unsheltered from the wind curl (Holland et al., 1984; Nakamura, 2006; Liu et al., 2021). Also consistent with the strong mixing regime, this homogenized PV zone expands to the whole subtropics with improving resolution, in contradiction to the weak mixing regime considered by Rhines & Young (1982). The erasure of the closed streamline bounding the homogenized PV (Cox, 1985) is consistent with observed tracer distribution, which exhibits no such internal boundary (Sarmiento, 1983). We plot in Fig. 2 the warm-layer PV profiles taken from Liu et al. (2021) for coarse- and fine-grained calculations, representing the laminar and eddying regimes, with the thin dashed lines marking the outcrops. It is seen that the PV in the eddying regime is strongly homogenized with its range reduced to about 20% of its laminar counterpart, which agrees with the earlier estimate of $\varepsilon_P \sim .2$. The hydrodynamic model of Hurlburt & Hogan (2000) shows an explosion of

345 eddies when the grid spacing is reduced to 3 km, but even such fine grids may not fully resolve
346 PV filaments indicative of the chaotic advection, a process that is particularly effective in mixing
347 the basin-wide PV. In other words, while the PV mixing is palpable in current numerical mod-
348 els, one expects an even higher degree of PV homogenization in the actual ocean.

349 For the observational evidence of homogenized PV, Stommel (1965, his Fig. 66) first no-
350 ticed that the thermocline in the subtropics deepens linearly with the latitude, rendering a colum-
351 nar PV that is "nearly constant". Across strong boundary currents where the relative vorticity
352 needs to be included, the columnar PV again is nearly uniform (Stommel, 1965, his Fig. 65;
353 Toole et al., 1990). The isopycnal PV (IPV) maps show that its upper thermocline value (corre-
354 sponding to our columnar PV) is discernibly homogenized throughout the subtropics (Holland et
355 al., 1984). The meridional section (McDowell et al., 1982, their Fig. 15) shows that the IPV iso-
356 lines above the main thermocline ($\sigma_\theta \leq 27$) generally parallel isopycnals in the subtropics; such
357 paralleling implies that thicknesses of the isopycnal layers increase with the Coriolis parameter,
358 so is their sum marking the thermocline depth --- hence consistent with Stommel's (1965) find-
359 ings. It should also be noted that since the PV homogenization is a synoptic feature, it would be
360 degraded in climatological maps (Lozier et al., 1995) due to decadal variability, a well-recog-
361 nized problem in mapping water-mass properties hence the PV (McCartney, 1982, his Section
362 3a).

363 To recap, given the short eddy mixing time, we estimate that the PV range would be re-
364 duced to a small fraction of its laminar range. We argue that the differential wind is weaker than
365 the differential heating in relative terms, so if one were to accept the two-layer approximation of
366 the ocean, it is only logical that the PV be assumed homogenized in the warm layer. We then

provide computational support from eddy-resolving numerical models and the observational evidence that can be gleaned from PV maps and sections. It is a misconception that the PV is homogenized only in the recirculation zone of the North Atlantic, which is attributable to the theoretical construct based on the laminar dynamics (Rhines & Young, 1982) and which simply does not comport with observations.

## 5. Upper-bound GOC

Homogenization of the PV has reduced its spatial distribution to a single value hence specified by the mean thermocline depth, but despite this extreme reduction in the degrees of freedom, we shall show that the resulting upper-bound GOC still entails enough structure to replicate the observed GOC. The deduced structure is summarized in Fig. 3, which consists of an interior of weak flow (*a*), strong flows along the subtropical front (*b*), the equator (*c*) and meridional boundaries (*d*), a recirculation in the northwest corner (*e*) and the MOC (*f*); the letters correspond to the following section headings.

For simplicity, we consider a beta plane, so the Coriolis parameter is synonymous with the latitudinal distance, and the solution given below has been nondimensionalized by scales defined by the prior constraints (also listed in Appendix B).

### *a. Interior*

In the interior where the relative vorticity is negligible (to be checked later), a homogenized PV implies that the thermocline deepens linearly with the latitudinal distance. We define therefore the depth scale by its maximum $[h] \equiv 2\bar{h}$ just south of the frontal jet, and $[P] \equiv f_1/[h]$

($f_1$ being the Coriolis parameter at the outcrop) so that the nondimensionalized PV has a unit magnitude. Defining additionally $[u] \equiv (g'[h])^{1/2}$, the homogenized PV then states

$$P = 1 = (y - \varepsilon u_y)/h \tag{22}$$

where the subscript *y* denotes the derivative and $\varepsilon \equiv r_c/l$ with $r_c \equiv (g'[h])^{1/2} {f_1}^{-1}$ being the deformation radius. Since $\varepsilon \approx .01$ (see Appendix B), it supports the neglect of the relative vorticity in the interior so that

$$h = y, \tag{23}$$

as shown in Fig. 4. This poleward deepening of the thermocline until its abrupt surfacing across a narrow frontal jet is a well-observed feature (McCartney, 1982), which however departs sharply from that based on the Sverdrup dynamics (Section 6.3). Assuming the zonal current to be geostrophic, it is given by

$$u = -\varepsilon h_y/y \tag{24}$$

$$= -\varepsilon/y. \tag{25}$$

Physically, a deepening thermocline causes a weak westward geostrophic flow, which intensifies toward low latitudes due to decreasing Coriolis parameter, the latter can be identified with the north equatorial current (NEC). There is no singularity as *y* approaches zero since, as we shall see later, there is an equatorial boundary layer where the equatorial undercurrent (EUC) resides.

Setting the scale of the stream function $[\psi] = [h][u]r_c$, it satisfies

$$\psi_y = -\varepsilon^{-1} h u \tag{26}$$

$$= 1; \tag{27}$$

that is, owing to the opposite latitudinal variation of the thermocline depth and zonal flow in the interior, the zonal transport per unit latitudinal distance is uniform and its interior total is unity,

$$[\psi]_0^1 = 1. \tag{28}$$

*b. Frontal Jet*

Along the outcrop, there is an eastward geostrophic jet, which can be identified with the Gulf Stream extension (GSE). The following solution is well known (see for example, Stommel, 1965, Chapter 8), but is matched here to the interior solution to be uniquely specified. Defining a stretched coordinate $\varsigma \equiv \varepsilon^{-1}(1 - y)$, the homogenized PV (Eq. 22) and the geostrophic balance (Eq. 24) state that

$$h = 1 + u_\varsigma, \tag{29}$$

$$u = h_\varsigma, \tag{30}$$

respectively, which have the solution

$$u = \exp(-\varsigma), \tag{31}$$

$$h = 1 - \exp(-\varsigma), \tag{32}$$

as seen in Fig. 4 where the boundary-layer width has been magnified 21 times (that is, if unmagnified, the front would be aligned with $y = 1$). The transport of the frontal jet can be seen from Eqs. (30) and (32) to be

$$[\psi]_0^\infty = \int_0^\infty hu \, d\varsigma$$

$$= \int_0^\infty h h_\varsigma \, d\varsigma$$

$$= 1/2, \tag{33}$$

hence it accommodates only half of the westward interior transport (Eq. 28).

For standard parameters, the frontal jet has an e-folding width 40 km with maximum speed 3.6 $m\ s^{-1}$ and transport 72 Sv, all are of the same order as the observed GSE (Johns et al., 1995). As we shall see later, this transport would be boosted by the recirculation and the MOC to improve the observational comparison. It is important to note that since the frontal jet is fully specified by the prior constraints via balances on a meridional plane, its properties are independent of the basin width, in sharp contrast to that based on the Sverdrup dynamics (Section 6.3).

*c. Equatorial Undercurrent*

Setting the stream function to zero at the outcrop, Eqs. (27) and (33) imply that, in the interior,

$$\psi = y - 1/2; \tag{34}$$

the westward interior flow thus bifurcates at $y = 1/2$ (about $20^0 N$) to form counter-rotating sub-tropical (anticyclonic) and tropical (cyclonic) gyres, the latter giving rise to the EUC. Physically, since the frontal jet along the outcrop is subjected to a local Coriolis parameter that is twice the interior average yet spans the same (full) thermocline depth, it can only return half the interior transport, the other half must return via the EUC. This bifurcation of the NEC is well observed in the western Pacific (Toole et al., 1990) with the northern and southern branches corresponding to the Kuroshio the Mindanao currents, respectively. In the western Atlantic, on the other hand, the bifurcation is complicated by the non-meridional orientation of the boundary hence the dominance of the North Brazil Current (Hazeleger et al., 2003).

For the equatorial boundary layer where the EUC resides, the homogenized PV (Eq. 22) and geostrophy (Eq. 24) again combine to yield (Pedlosky, 1991)

$$u_{yy} - \varepsilon^{-2} y u = \varepsilon^{-1}. \tag{35}$$

Defining a stretched coordinate $\varsigma \equiv \varepsilon^{-2/3} y$, then to the accuracy of O ($\varepsilon^{1/3}$), Eq. (35) becomes

$$u_{\varsigma\varsigma} - \varsigma u = 0, \tag{36}$$

which has the solution

$$u = C \cdot Ai\,(\varsigma), \tag{37}$$

$$h = -\varepsilon^{1/3} C \cdot Ai'(\varsigma). \tag{38}$$

To determine the constant *C*, we note that the Bernoulli function

$$B \equiv h + u^2/2 \tag{39}$$

457 satisfies, subjected to Eqs. (22), (24) and (26),

458 $$B_\psi = 1, \tag{40}$$

459 which yields

460 $$B = 1/2 + \psi, \tag{41}$$

461 given its value at the outcrop (from Eqs. [31] and [32]). Since at the equator, $\psi = 0$ hence $B =$
462 $1/2$, it yields $C \approx 2.41$. The solution for the equatorial boundary layer is shown in Fig. 4 with
463 its width magnified by 5 (that is, without the magnification, the equator would be aligned with
464 $y = 0$). It should be noted that the Bernoulli function being a constant along a streamline is not
465 due to its conservation, which would not apply in an eddying ocean, but the outcome of PV ho-
466 mogenization and geostrophic balance.

467 Although the EUC was initially suggested to be driven by the easterly trades (Charney,
468 1960), its subtropical source is subsequently established from tracer observation (Fine et al.,
469 1987; Johnson & McPhaden, 1999) and numerical calculations (Goodman et al., 2005). Ped-
470 losky (1991) has formulated an inertial model of the EUC, which however requires a prescription
471 of the bifurcation latitude. In our formulation however, the EUC is an internal component of the
472 gyre circulation hence fully specified by the prior constraints.

473 Based on standard parameters, the model EUC would extend to about $2^0 N$, as observed
474 (Wyrtki & Kilonsky, 1984). It has a speed of 3 $m\ s^{-1}$ and a hemispheric transport of 72 Sv
475 (hence a total transport of 144 Sv), both are high compared with their observed values, which

however would be reduced by the presence of a tropical layer, a prominent feature of the observed ocean. The tropical circulation driven by an easterly trade has been simulated realistically based on the laminar dynamics (Chen et al., 1994), which can be appended to our upper-bound circulation. It however has strong effect on the EUC, as seen in the schematic of Fig. 5 and discussed below.

We note first that the tropical layer (Polka-dotted) would depress the main thermocline downward as the warm layer thickness is constrained by the homogenized PV. Since the Bernoulli function at the equator, being set by its outcrop value, remains unchanged, one sees immediately that the EUC would be weakened. As an example, for a tropical layer thickness of 160 m (or non-dimensionally $h_s$ =.16), the boundary condition to the solution Eqs. (37) and (38) would be

$$h + u^2/2 = 1/2 - h_s = .34 \text{ at } \varsigma = 0, \tag{42}$$

which yields $C$ = 1.76. The EUC thus is weakened from 3 to 2.3 $m\ s^{-1}$, a 23% reduction. As regards the EUC transport, a tropical layer extending to $10^0$N, for example, would reduce its subtropical supply by half from 72 to 36 Sv. And then the northern subsurface countercurrent (NSCC, Tsuchiya, 1972) would syphon the transport from the southward boundary current, a feature that is well discerned in tritium transects showing double cores associated with the NSCC and EUC in addition to its source in the NEC (Fine et al., 1987, their Fig. 6). If we set the NSCC transport at 10 Sv (Wyrtki & Kilonsky, 1984), it would further reduce the hemispheric supply of the EUC from the foregoing 36 to 26 Sv, resulting in a total EUC transport of 52 Sv. This represents a 2/3 reduction from that estimated earlier in the absence of the tropical layer, which is now commensurate with its observed transport.

*d. Meridional Boundary Current*

With the zonal flow determined in the interior, the meridional boundary currents represent merely passive conduits forced by mass continuity. Along the western boundary, we define a stretch coordinate $\varsigma \equiv \varepsilon^{-1}x$, then the homogenized PV and geostrophy imply, respectively,

$$h = y + v_{\varsigma}, \tag{43}$$

$$yv = h_{\varsigma}. \tag{44}$$

It has the solution

$$v = Aexp(-\sqrt{y}\varsigma), \tag{45}$$

$$h = y - \sqrt{y}A\ exp(-\sqrt{y}\varsigma), \tag{46}$$

where

$$A = \sqrt{y} - \sqrt{1-y} \tag{47}$$

by applying Eq. (41) and $\psi = 0$ along $x = 0$.

The solution is shown in Fig. 5 in dashed lines, noting that the meridional flow is of opposite sign on two sides of the bifurcation (the reason for showing only the speed), and they are reversed along the eastern boundary. Unlike the interior thermocline that deepens monotonically with the latitude until it surfaces abruptly across a narrow frontal jet, the thermocline along the western boundary shoals gradually away from its maximum mid-latitude depth. This would lead to crowding of depth contours in the northwest corner of the subtropical gyre, as is the observed

case (Stommel, 1965, his Fig. 66). Since the boundary layer is scaled by the deformation radius, it narrows with the latitude, and the southern branch has deeper thermocline at the coast than the interior; both these features are consistent with observation in the western Pacific (Toole et al., 1990, their Fig. 10).

Being a receptacle of the mass continuity, there is no prohibition of the eastern boundary current (EBC), whose allowance is more compliant with its observed prominence (Talley et al., 2011). This is in sharp contrast to the laminar regime when the EBC is prohibited by the frictional vorticity balance, which has other unrealistic consequences: without the meridional flow, the normal flow would be geostrophic, and its vanishing at the boundary renders a level thermocline, which thus must be situated at the surface if it outcrops to the north --- a singularity unobserved in the ocean. In an eddying ocean, on the other hand, the PV homogenization has voided the frictional vorticity balance, and the thermocline depth would counter-vary with the boundary current on account of the constant Bernoulli function.

*e. Recirculation*

We now show that the PV homogenization necessitates the generation of a recirculation as the western boundary current (WBC) separates from the meridional boundary and morphs into a frontal jet, whose physics can be gleaned from Fig. 6. Because of the homogenized hence finite PV, the WBC can depart the boundary only at a tangent, which then curls increasingly negatively due to the beta effect until it turns south; after that, the trend reverses with the acquisition of the positive curvature, resulting in a meandering path. Because of the invariable dissipation and blurring of the thermal front, the initial arc is the most sharply defined. Within this arc, the homogenized PV would continue to deepen the thermocline as in the subtropical interior

538 (striped) and, also like the interior, the sloping thermocline would induce a westward geostrophic
539 flow --- except this flow is now blocked by the arc to recirculate through the frontal jet, thus en-
540 hancing its transport.

541 Since the recirculation is couched within the arc, we need to first determine its trajectory.
542 Ou and Ruijter (1986) have solved a similar problem of the retroflected Agulhas Current. Their
543 derivation however needs to be modified to incorporate the homogenized PV, and then some
544 simplifications are employed for the following derivation.

545 In the interior of the warm arc, the thermocline depth and stream function are given by
546 Eqs. (23) and (34), respectively, which provide the far-field conditions for the frontal jet. As-
547 suming a "narrow-jet" (checked later), we use the natural coordinate affixed to the outcrop with $\varsigma$
548 being the spanwise distance scaled by the deformation radius. Including the flow curvature, the
549 homogenized PV and the spanwise momentum balance are generalized to

550 $$h = y + v_\varsigma + \varepsilon c v, \tag{48}$$

551 $$yv + \varepsilon c v^2 = h_\varsigma, \tag{49}$$

552 where $v$ is the downstream velocity and the curvature $c$ has been scaled by $l^{-1}$. Assuming
553 "small-amplitude" meander (also checked later)

554 $$y = 1 + y', y' \ll 1, \tag{50}$$

555 we multiply Eq. (49) with $h$, integrate it across the jet and apply the far-field conditions Eqs. (23)
556 and (34) to derive

$$c = -y'/(2m), \tag{51}$$

where

$$m \equiv \varepsilon \int_0^\infty hv^2 d\varsigma \tag{52}$$

is the momentum flux carried by the frontal jet. On account of Eq. (50), this momentum flux can be approximated by its value at the separation point and, by applying the solution Eqs. (31) – (32), we derive

$$m \approx \varepsilon/6, \tag{53}$$

so Eq. (51) yields

$$c \approx -3y'/\varepsilon. \tag{54}$$

We have thus determined the curvature of the jet as a function of its northward excursion, from which one may calculate its path.

Let $\theta$ be the tangential angle measured clockwise from north and $\eta$ the arc length, we have by definition

$$c = -d\theta/d\eta, \tag{55}$$

and with

$$d\eta = dy/\cos\theta, \tag{56}$$

we obtain

$$cdy = -d(sin\theta). \tag{57}$$

Integrating this equation from the initial orientation $\theta = 0$, we derive

$$\sin\theta = -\int_0^{y'} cdy'$$

$$= 3(2\varepsilon)^{-1}y'^2, \tag{58}$$

which allows the calculation of the jet path.

Our primary concern is the poleward extent of the initial arc where $\theta = \pi/2$, which yields

$$y'_{max} = (2\varepsilon/3)^{1/2} \approx 0.082. \tag{59}$$

Inserting the scale definitions into Eq. (59), the dimensional distance is

$$y_{max} \approx .82(r_c l)^{1/2}. \tag{60}$$

It is seen that since both baroclinicity and the beta effect play controlling roles in the jet path, the latter is scaled by the geometric mean of the deformation radius and the warm-layer extent. Moreover, as the two differ by two orders of magnitude (40 versus 4000 km), the meandering scale is of order 400 km, justifying therefore both the "narrow-jet" and the "small-amplitude" approximations used in the derivation.

With the constant transport increment Eq. (27), the recirculation would increase the GSE transport in proportion to its northward excursion, which is thus substantial. As the recirculation takes on the PV of the warm layer and is framed within the arc --- itself a function only of this

PV, the recirculation is an integral part of the subtropical gyre hence fully specified by the prior constraints. This contrasts sharply the previous recirculation models, which require prescribing its PV and/or spatial confinement (Cessi, 1988; Marshall & Nurser, 1988). On the other hand, since our recirculation is the outcome of the homogenized PV, it is eddy-driven, as conjectured previously (Niiler, 1986).

Qualitatively, the framing of our recirculation within the warm arc of the separated jet is consistent with the observational and computational evidence (Worthington, 1976; Jayne et al., 2009). And because the Kuroshio takes a more eastward path after separation due to the coastal orientation, one expects its recirculation to be less prominent than the GSE, as indeed the case. The deduced poleward increase of the jet transport is due solely to the deepening thermocline while the jet speed remains unchanged because of the Bernoulli law Eq. (41), both these features are consistent with observations (Knauss, 1978, his Fig. 8.3; Johns et al., 1995). According to Eq. (60), the arc extends 330 km beyond the separation latitude; since the westward transport per unit distance Eq. (27) is $3.6\times 10^{-2}$ Sv km$^{-1}$, the jet transport thus peaks at 84 Sv, 30% of which resides in the recirculation, supporting its well-subscribed importance (Richardson, 1985; Niiler, 1986; Johns et al., 1995; Jayne et al., 2009).

*f. Meridional Overturning Circulation*

As a prior constraint, we have determined the MOC due to the differential surface heating (Section 2). This MOC is a generalization of the laminar overturning cell to include random eddy exchange across the subtropical front (Lozier, 2010) and since the entrainment of cold eddies occurs primarily near where the GSE separates from the boundary and warm eddies are shed usually after the initial arc, the derived MOC would fully augment the peak transport of the GSE,

raising it from 84 to 106 Sv, thus improving its observational comparison (Johns et al., 1995). Boosted by the recirculation and the MOC, the subtropical gyre thus is western-intensified, even without the operation of the laminar Sverdrup dynamics.

It is worth emphasizing the fundamental difference of the MOC of a laminar and eddying ocean. In the laminar regime, it requires external ME source, including the APE, to cross the potential energy barrier hence can be said to be mechanically driven (Huang, 1999; Hughes et al., 2009). In an eddying ocean, on the other hand, the MOC is propelled by fluctuations of a NT system toward the MEP and the external ME source only regulates the thermocline depth (Eq. 12) without impacting the MOC.

One key element of our upper-bound GOC is its internal coupling to the MOC, which takes qualitatively different forms between the laminar and eddying regimes. While stronger wind expectedly drives a stronger GOC, it is through the wind curl in a laminar regime, but in an eddying ocean it is through the wind work that deepens the thermocline (Eq. 12). The effect of the buoyancy forcing is still more nuanced, for which we need to first point out a significant shortfall of the widely used restoring condition that is not sufficiently recognized: a stronger air-sea exchange, for example, would increase the stratification (toward the restoring temperature) but has the opposite effect in a coupled ocean/atmosphere forced by the radiative heating (as seen from the temperature scale in Appendix B). In a laminar regime therefore, stronger air-sea exchange would enhance both the MOC and subtropical gyre; but in an eddying ocean, the augmented MOC would shoal the thermocline (Eq. 12) and together with the weaker stratification noted above, the subtropical gyre would doubly weaken. In other words, the MOC actually counter-varies with the GOC in an eddying ocean when air-sea exchange coefficient changes, as

636 seen in eddy-resolving calculations (Hogg & Gayen, 2020, their Fig. 4 when the stratification
637 hence the deformation radius is substantially greater than the grid spacing). Since the MOC
638 would add to the GSE transport, this counter variation may somewhat stabilize the peak GSE
639 transport.

640 *g. Upper bound*

641 The PV homogenization steepens the interior thermocline to maximize its depth just
642 south of the outcrop. As this depth enters the dynamical scaling of the gyre circulation, the de-
643 rived GOC thus represents an upper bound hence the title of the paper.

644 This inference of an upper-bound GOC is consistent with GCM experiments, which show
645 that increasing the spatial resolution hence eddy mixing of the PV indeed leads to a stronger
646 GOC, as manifested in the mean kinetic energy (Bryan et al., 2007, their Fig. 3). This tendency
647 points to the obvious falsity of parameterizing the eddy effect by an eddy diffusivity in the mo-
648 mentum equation, which would smooth the relative vorticity to weaken the GOC (e. g. Munk,
649 1950). The use of the eddy diffusivity is justified only when it is applied to the macroscopic PV,
650 as seen in Eq. (14); and to capture the eddy effect from primitive equation models, there is no
651 substitute than resolving the eddies.

652 The PV homogenization has removed the PV gradient that anchors the Sverdrup flow
653 (Eq. 14), and it has short-circuited the effect of the wind curl so the wind forcing enters only
654 through the mechanical work it imparts to the ocean (Eq. 12). As such, the upper-bound GOC
655 retains no vestige of the Sverdrup balance, and its reproduction of the observed GOC can only be

ascribed to the PV mixing. In the next section, we shall reassess the Sverdrup balance in an eddying ocean and highlight the difference between laminar and eddying regimes.

## 6. Laminar versus Eddying Dynamics

The Sverdrup balance is based on the laminar dynamics as it predates the satellite observation of teeming eddies, but given the well-demonstrated importance of eddies in mixing the PV, the contrasts of the two regimes on theoretical, computational, and observational bases merit further discussion, as provided below.

### 6.1 Theoretical Basis

The Sverdrup balance is a local balance, yet its applicability hinges on the presence of remote meridional boundaries as there obviously can be no Sverdrup flow in a circumpolar ocean. This logical difficulty is absent from our model for which the thermal properties are determined by balances on a meridional plane hence independent of the meridional boundaries. The presence of the latter only acts to channel meridional boundary currents and the EUC via the mass continuity, and the recirculation via the PV homogenization.

Another unwanted singularity readily emerges from the ventilated thermocline theory (Luyten et at., 1983). Since the laminar dynamics excludes the EBC, the zonal flow is geostrophic near the eastern boundary to yield level isopycnals, so isopycnals above the main thermocline, which necessarily outcrop in the subtropics, would all merge at the surface along the eastern boundary. This singular feature obviously is unobserved in the ocean and its remedy remains contrived (Pedlosky, 1983). In our formulation however, the PV mixing has voided the

676 frictional vorticity balance to allow the EBC and hence varying isopycnal depth, which naturally
677 removes the above singularity.

678 While the ventilated thermocline theory has illustrated the laminar constraint on the sub-
679 ducted flow, it is not a theory of the GOC as it does not address the closed subtropical gyre,
680 which is largely unsheltered from the surface wind. Our upper-bound GOC on the other hand
681 depicts closed circulation, and since the PV mixing constitutes the higher order term in the vorti-
682 city balance (Eq. 14), the Sverdrup flow, if manifests, represents merely a regular perturbation of
683 --- hence does not materially alter --- the upper-bound GOC.

684 The inertial model of Marshall & Nurser (1986) falls in the laminar regime, differing
685 from the Sverdrup dynamics in its inclusion of the relative vorticity. Since the latter is negligible
686 in the ocean interior, the inertial balance there is voided by the PV mixing, just like the Sverdrup
687 balance; then being a quasi-geostrophic model, it contains no outcrop to fall short as a model of
688 the GOC (Section 1). Its application to the recirculation is better justified, and the role of the PV
689 mixing is that the PV may not be assigned different values along individual streamlines (Cessi,
690 1988) as the higher-order frictional balance invoked to constrain these values (Marshall &
691 Nurser, 1986) would be nullified by the PV mixing. In other words, the inertial balance is sub-
692 sumed by the PV homogenization, and the resulting flow is not just a particular solution to the
693 inertial gyre, but its only justifiable solution in an eddying ocean.

694 **6.2 Computational Basis**

695 Coarse-grain numerical calculations have replicated many features of the ventilated ther-
696 mocline theory, including homogenized PV in the northwest subtropics bounded by a closed

streamline (Cox, 1985). Eddy-resolving calculations however show that the homogenized PV would expand to the whole subtropics, erasing in effect the internal boundary unobserved in the tracer distribution. This led Böning & Cox (1988) to surmise that the expanded PV homogenization is the outcome of different physics from that posited by Rhines & Young (1982), which requires weak eddy mixing to preserve the PV conservation along closed streamline (Section 4). Our postulate of the PV homogenization hinges on conservation of only the microscopic PV, which can only be aided by strong mixing hence free from the weak mixing constraint. Unfortunately, the weak mixing regime has contributed to the still-held misconception that the PV is homogenized only in the recirculation zone. In the parlance of the ventilated thermocline theory, the PV homogenization has morphed the geostrophic contours into a geostrophic plateau to no longer constrain the mean flow; it reduces the hyperbolic problem of intricate circulation pattern to an elliptic one of simple structure.

The finer grain calculations have improved simulation of the subtropical gyre, including stronger GSE and its proper separation from the western boundary (Smith et al., 2000; Bryan et al., 2007; Chassignet & Xu, 2017), yet it is accompanied by shrinkage of the Sverdrup balance to isolated patches (Holland & Rhines, 1980). These opposite trends clearly downgrade the relevance of the Sverdrup balance to the improved mean flow, which must be attributed to stronger PV mixing by the resolved eddies.

### 6.3 Observational Basis

Since the Sverdrup flow only reaches O (1 $cm\ s^{-1}$), it cannot be discerned amidst the eddying motion. As such, its observational supports are derived from the implied transport, which involves adjusting level-of-no-motion or integration depth to produce a match (Hautala et al.,

719 1994; Wunsch, 2011; Gray & Riser, 2014). Since it amounts to setting a barotropic velocity of
720 the same order as the Sverdrup flow, the uncertainty in differentiating the latter cannot be over-
721 come simply by calculating the transport. In contrast, the homogenized PV can be gleaned di-
722 rectly from hydrographic data (Section 4), which provides a tangible observational support.

723 In addition, the Sverdrup dynamics and PV homogenization make different predictions
724 that are testable by observations; a few obvious ones are listed below.

725 • Being a local balance, the Sverdrup transport increases with the basin width (Hellerman
726 & Rosenstein, 1983), yet the Kuroshio is comparable to the Gulf Stream (GS) in transport
727 despite a basin that is more than twice wider (Hall, 1989). In contrast, our frontal jet is
728 constrained by properties on a meridional plane regardless the basin width, which may
729 explain the above observation.
730 • Although the Sverdrup transport at the latitude of maximum wind curl can match the ob-
731 served GS transport if one includes the MOC (Leetmaa et al., 1977; Schmitz et al., 1992),
732 the agreement is fortuitous since the Sverdrup transport would decrease to the north while
733 the observed GS transport increases unabated to several times the maximum Sverdrup
734 transport. Part of the increase is attributable to recirculation, which however is unrelated
735 to --- hence makes no commentary on the validity of --- the Sverdrup balance. In con-
736 trast, our western boundary current is fed continually by the interior flow all the way to
737 its separation and beyond, reaching a maximum at its northernmost reach, just as ob-
738 served (Fig. 3).

- According to the Sverdrup dynamics, the thermocline is the deepest at the maximum wind-curl (about $20^0$N), which shoals gradually to the north (Welander, 1968). The observed thermocline however deepens continually with latitude until it reaches the GSE when it outcrops abruptly (McCartney, 1982), just as predicted by the homogenized PV.

To recap, we argue that any objective reading of the observational evidence would favor the homogenized PV over the Sverdrup balance. That our explanation of the GOC in an eddying ocean remains entrenched in the Sverdrup dynamics can be attributed to the lack of a theoretical framework that incorporates the central role played by eddies yet depicts explicit closed circulation. By considering the asymptotic state of infinite eddy mixing, the upper-bound GOC can be derived unambiguously, whose resemblance to the observed one suggests that it may provide an alternative paradigm in our conception of the GOC.

## 7. Conclusion

In this second part of a two-part paper, we consider the GOC within the deductive framework of our climate theory. With the climate being a macroscopic manifestation of an NT system, we have invoked the MEP for its closure, which has reduced the ocean to warm and cold watermasses and determined bulk properties of the thermocline --- the prior constraints for the present dynamical derivation.

Consistent with the asymptotic thermal state, we assume the PV to be homogenized in the warm layer, and the resulting upper-bound GOC has reproduced the salient features of the observed one, including the western intensified subtropical gyre and counter-rotating tropical gyre feeding the EUC. The quantitative agreements suggest that the PV homogenization may provide

an alternative explanation of the GOC in an eddying ocean in place of the laminar Sverdrup dynamics.

Together with Part 1 on the GAC, we see that the PV homogenization may unify the large-**scale** dynamics of both planetary fluids, based on which we posit that the general planetary circulations represent the maximum macroscopic flow extractable by microscopic stirring --- within the confine of the thermal differentiation.


## Acknowledgments

I have benefitted from discussions with Dake Chen, Ryan Abernathey and Tongya Liu. This research has not received any specific grant from funding agencies in the public, commercial, or not-for-profit sectors.


## Data Availability Statement

This paper contains no propriety data.

## APPENDIX A

### Acronyms

EBC Eastern boundary current

EUC Equatorial undercurrent

GAC General atmosphere circulation

GCM General circulation model

778 GOC General ocean circulation

779 GS Gulf Stream

780 GSE Gulf Stream extension

781 IPV Isopycnal potential vorticity

782 ITCZ Inter-tropical convergence zone

783 ME Mechanical energy

784 MEP Maximum entropy production

785 MOC Meridional overturning circulation

786 NEC North equatorial current

787 NSCC Northern subsurface countercurrent

788 NT Nonequilibrium thermodynamics

789 PV Potential vorticity

790 WBC Western boundary current

791 APPENDIX B

792 **Symbols and standard values**

793 $B$ Bernoulli function

794 $C_{p,o}$ Specific heat of ocean ($= 4.2 \times 10^3\ J\ Kg^{-1}\ {}^0C^{-1}$)

795 $f_1$ Coriolis parameter at outcrop ($= .9 \times 10^{-4}\ s^{-1}$)

796 $g'$ Reduced gravity ($= 1.3 \times 10^{-2}\ m\ s^{-2}$)

797 $h$ Thermocline depth

798 $h_m$ Mixed layer depth ($=220\ m$)

799 $\bar{h}$ Mean thermocline depth (=.5 km)

800 $[h]$ Thermocline depth scale ($=2\ \bar{h}$=1 km)

801 $k$ Eddy diffusivity ($= 5 \times 10^4\ m^2\ s^{-1}$)

802 $K$ MOC flux ($=3.6\ m^2\ s^{-1}$)

803 $K_E$ Ekman flux at outcrop ($=1.1\ m^2\ s^{-1}$)

804 $L$ Hemispheric basin length (=8000 km)

805 $l$ Warm-layer extent ($=L/2$=4000 km)

806 $P$ Columnar potential vorticity

807 $[P]$ PV scale ($= f_1/[h] = .9 \times 10^{-7}\ m^{-1}\ s^{-1}$)

808 $q$ Absorbed solar flux

809 $\Delta q$ Range of $q$ ($= 300\ W\ m^{-2}$)

810 $r_C$ Deformation radius ($= (g'[h])^{1/2}/f_1 = 40$ km)

811 $t_m$ Warm layer mixing time (=10 y)

812 $t_r$ Ocean restoring time (=4.4 y)

813 $t_s$ Sverdrup time (=50 y)

814 $T$ Ocean temperature (global-mean removed)

815 $[T]$ Temperature scale ($= \alpha^{-1}\Delta q = 20\ ^0C$)

816 $\Delta T$ Differential ocean temperature ($= 10\ ^0C$)

817 $u$ Zonal current

818 $[u]$ Velocity scale ($=(g'[h])^{1/2} = 3.6\ m\ s^{-1}$)

819 $v_s$ Sverdrup flow ($= 2.5 \times 10^{-3}\ m\ \ s^{-1}$)

820 $y$ Latitudinal distance

821 $[y]$ Distance scale ($= l = 4000$ km)

822 $\alpha$ Air-sea exchange coefficient ($= 15\ W\ m^{-2}\ ^0C^{-1}$)

823 $\beta$ gradient of Coriolis parameter ($= 2 \times 10^{-11}\ m^{-1}\ s^{-1}$)

| | | |
|---|---|---|
| 824 | $\varepsilon$ | the ratio $r_c/l$ $(= 0.01)$ |
| 825 | $\varepsilon_P$ | Laplacian of PV (=.2) |
| 826 | $\varepsilon_T$ | Laplacian of temperature (=2.3) |
| 827 | $\gamma$ | Air-sea exchange velocity $(= 3.6 \times 10^{-6}\ m\ s^{-1})$ |
| 828 | $\nu$ | Vertical diffusivity $(= 10^{-4}\ m^2\ s^{-1})$ |
| 829 | $\rho_o$ | Ocean density $(= 10^3\ Kg\ m^{-3})$ |
| 830 | $\sigma$ | Entropy production |
| 831 | $\tau^*$ | Wind Stress |
| 832 | $\tau$ | Wind stress per unit water density $(= \tau^*/\rho_o)$ |
| 833 | $\tau_1$ | Magnitude of $\tau$ at outcrop $(= 10^{-4}\ m^2\ s^{-2})$ |
| 834 | $\Delta\tau$ | Range of $\tau$ over warm layer $(= 10^{-4}\ m^2\ s^{-2})$ |
| 835 | $[\psi]$ | Transport scale $(= [h][u]r_c = 144\ Sv)$ |

836 REFERENCES


837 Auer, S. J., 1987: Five-year climatological survey of the Gulf Stream system and its associated

838 rings. *J. Geophys. Res.*, **92**, 11709–11726, doi.org/10.1029/jc092ic11p11709

839 Berloff, P., McWilliams, J., and A. Bracco, 2002: Material transport in oceanic gyres. Part I:
840 Phenomenology. *J. Phys. Oceanogr.*, **32**, 764–796, doi.org/10.1175/1520-
841 0485(2002)032<0764:mtiogp>2.0.co;2

842 Böning, C. W., and M. D. Cox, 1988: Particle dispersion and mixing of conservative properties
843 in an eddy-resolving model. *J. Phys. Oceanogr.*, **18**, 320-338, doi.org/10.1175/1520-
844 0485(1988)018<0320:pdamoc>2.0.co;2

845 Bower, A. S., and N. B. Hogg, 1996: Structure of the Gulf Stream and its recirculation at 55 W.
846 *J. Phys. Oceanogr*., **26**, 1002-1022, doi.org/10.1175/1520-0485(1996)026<1002:sot-
847 gsa>2.0.co;2

848 Brown, M. G., and K. B. Smith, 1991: Ocean stirring and chaotic low-order dynamics. *Phys.*
849 *Fluids*, **A3**, 1186-1192, doi.org/10.1063/1.858047

850 Bryan, F. O., Hecht, M. W., and R. D. Smith, 2007: Resolution convergence and sensitivity stud-
851 ies with North Atlantic circulation models. Part I: The western boundary current system.
852 *Ocean Modelling*, **16**(3), 141-159, doi.org/10.1016/j.ocemod.2006.08.005

853 Cessi, P., 1988: A stratified model of the inertial recirculation. *J. Phys. Oceanogr.*, **18**, 662-682,
854 doi.org/10.1175/1520-0485(1988)018<0662:asmoti>2.0.co;2

855 Charney, J. G., 1960: Non-linear theory of a wind-driven homogeneous layer near the Equator.
856 *Deep-Sea Res.,* **6**, 303–310, doi.org/10.1016/0146-6313(59)90089-9

857 Chassignet, E. P., and X. Xu, 2017: Impact of horizontal resolution (1/12° to 1/50°) on Gulf
858 Stream separation, penetration, and variability. *J. Phys. Oceanogr*., **47**(8),1999-2021,
859 doi.org/10.1175/jpo-d-17-0031.1

860 Chelton, D. B., Schlax, M. G., Samelson, R. M., and R. A. de Szoeke, 2007: Observations of
861 large oceanic eddies. *Geophys. Res. Lett*., **34**, L15606, doi:10.1029/2007GL030812

862 Chen, D., Rothstein, L. M., and A. J. Busalacchi, 1994: A hybrid vertical mixing scheme and its
863 application to tropical ocean models. *J. Phys. Oceanogr*., **24**(10), 2156-2179,
864 doi.org/10.1175/1520-0485(1994)024<2156:ahvmsa>2.0.co;2

865 Colin de Verdière, A., 1988: Buoyancy driven planetary flows. *J. Mar. Res*., **46**(2), 215-265,
866 doi.org/10.1357/002224088785113667

867 Colin de Verdière, A., 1989: On the interaction of wind and buoyancy driven gyres. *J. Mar. Res*.,
868 **47**(3), 595-633, doi.org/10.1357/002224089785076172

869 Cox, M., 1985: An eddy resolving numerical model of the ventilated thermocline. *J. Phys.*
870 *Oceanogr*., **15**, 1312-1324, doi.org/10.1175/1520-0485(1985)015<1312:aernmo>2.0.co;2

871 Ferrari, R., and C. Wunsch, 2009: Ocean circulation kinetic energy: Reservoirs, sources, and
872 sinks. *Annu. Rev. Fluid Mech.*, **41**, 253–282, doi.org/10.1146/an-
873 nurev.fluid.40.111406.102139

874 Fine, R. A., Peterson, W. H., and H. G. Ostund, 1987: The penetration of tritium into the tropical
875 Pacific. *J. Phys. Oceanogr*., **17**, 553-564, doi.org/10.1175/1520-
876 0485(1987)017<0553:tpotit>2.0.co;2

877 Fofonoff, N. P., 1954: Steady flow in a frictionless homogeneous ocean. *J. Mar. Res*., **13**, 254-
878 262.

879 Fu, L.-L., Chelton, D. B., Le Traon, P.-Y., and R. Morrow, 2010: Eddy dynamics from satellite
880 altimetry. *Oceanography*, **23**(4),14–25, doi.org/10.5670/oceanog.2010.02

881 Gill, A. E., 1971: Ocean models. *Philos. Trans. R. Soc. London*, **(A)**270, 391-413.

882 Goodman, P. J., Hazeleger, W., de Vries, P., and M. Cane, 2005: Pathways into the Pacific Equa-
883 torial Undercurrent: A trajectory analysis. *J. Phys. Oceanogr.*, **35**(11), 2134-2151,
884 doi.org/10.1175/jpo2825.1

885 Gray, A. R., and S. C. Riser, 2014: A global analysis of Sverdrup balance using absolute geo-
886 strophic velocities from Argo. *J. Phys. Oceanogr.*, **44**, 1213–1229, doi.org/10.1175/jpo-d-
887 12-0206.1

888 Greatbatch, R., Zhai, X., Eden, C., and D. Olbers, 2007: The possible role in the ocean heat
889 budget of eddy-induced mixing due to air–sea interaction. *Geophys. Res. Lett.*, **34**, L07604,
890 doi:10.1029/2007GL029533

891 Hall, M. M., 1989: Velocity and transport structure of the Kuroshio extension at $35^0N$, $152^0E$. *J.*
892 *Geophys. Res.* (*Oceans*), **94**, 14,445-14,459, doi.org/10.1029/jc094ic10p14445

893 Haney, R. L., 1971: Surface thermal boundary condition for ocean circulation models. *J. Phys.*
894 *Oceanogr.*, **1**(4), 241-248, doi.org/10.1175/1520-0485(1971)001<0241:stbcfo>2.0.co;2

895 Harrison, D., 1981: Eddy lateral vorticity transport and the equilibrium of the North Atlantic sub-
896 tropical gyre. *J. Phys. Oceanogr.*, **11**, 1154–1158, doi.org/10.1175/1520-
897 0485(1981)011<1154:elvtat>2.0.co;2

Hautala, S. L., Roemmich, D. H., and W. J. Schmitz, 1994: Is the North Pacific in Sverdrup balance along 24° N? *J. Geophys. Res.* (*Oceans*), **99**(C8), 16041-16052, doi.org/10.1029/94jc01084

Hazeleger, W., de Vries, P., and Y. Friocourt, 2003: Sources of the Equatorial Undercurrent in the Atlantic in a high-resolution ocean model. *J. Phys. Oceanogr.*, **33**(4), 677-693, doi.org/10.1175/1520-0485(2003)33<677:soteui>2.0.co;2

Hellerman, S., and M. Rosenstein, 1983: Normal monthly wind stress over the world ocean with error estimates. *J. Phys. Oceanogr*., **13**, 1093-1104, doi.org/10.1175/1520-0485(1983)013<1093:nmwsot>2.0.co;2

Hilderbrand, F. B., 1962: *Advanced Calculus for Applications*. Englewood Cliffs, NJ, Prentice-Hall, Inc., 646 pp.

Hogg, N. G., 1992: On the transport of the Gulf Stream between Cape Hatteras and the Grand Banks. *Deep-Sea Res.*, **A39**, 1231-1246.

Hogg, A. M., and B. Gayen, 2020: Ocean gyres driven by surface buoyancy forcing. *Geophys. Res. Lett.*, **47**, e2020GL088539, doi.org/10.1002/essoar.10503133.1

Holland, W. R., and B. Lin, 1975: On the origin of mesoscale eddies and their contribution to the general circulation of the ocean. I. A preliminary numerical experiment. *J. Phys. Oceanogr.*, **5**, 642-657, doi.org/10.1175/1520-0485(1975)005<0642:otgome>2.0.co;2

Holland, W. R., and P. B. Rhines, 1980: An example of eddy-induced ocean circulation. *J. Phys. Oceanogr.*, **10**, 1010-1031, doi.org/10.1175/1520-0485(1980)010<1010:aeoeio>2.0.co;2

Holland, W. R., Keffer, T., and P. B. Rhines, 1984: Dynamics of the oceanic general circulation: the potential vorticity field. *Nature*, **308**, 698-705, doi.org/10.1038/308698a0

Huang, R. X., and G. R. Flierl, 1987: Two-layer models for the thermocline and current structure in subtropical/subpolar gyres. *J. Phys. Oceanogr.*, **17**(7), 872-884, doi.org/10.1175/1520-0485(1987)017<0872:tlmftt>2.0.co;2

Huang, R. X., 1999: Mixing and energetics of the oceanic thermohaline circulation. *J. Phys. Oceanogr.*, **29**(4),727-46, doi.org/10.1175/1520-0485(1999)029<0727:maeoto>2.0.co;2

Hughes, G. O., Hogg, A. M., and R. W. Griffiths, 2009: Available potential energy and irreversible mixing in the meridional overturning circulation. *J. Phys. Oceanogr.*, **39**(12), 3130–3146, doi.org/10.1175/2009jpo4162.1

Hurlburt, H. E., and P. J. Hogan, 2000: Impact of 1/8 to 1/64 resolution on Gulf Stream model–data comparisons in basin-scale subtropical Atlantic Ocean models. *Dyn. Atm. Oceans*, **32**(3-4), 283-329, doi.org/10.1016/s0377-0265(00)00050-6

Ierley, G. R. and W. R. Young, 1983: Can the western boundary layer affect the potential vorticity distribution in the Sverdrup interior of a wind-gyre? *J. Phys. Oceanogr.*, **13**, 1753-1763, doi.org/10.1175/1520-0485(1983)013<1753:ctwbla>2.0.co;2

Jayne, S., Hogg, N., Waterman, S., Rainville, L., Donohue, K., Watts, D., Tracey, K., McClean, J., Maltrud, M., Qiu, B., Chen, S., and P. Hacker, 2009: The Kuroshio extension and its recirculation gyres. *Deep-Sea Res.*, **56**, 2088–2099, doi.org/10.1016/j.dsr.2009.08.006

Jenkins, W. J., 1988: The use of anthropogenic tritium and helium3 to study subtropical gyre ventilation and circulation. *Phil. Trans. R. Soc. London*, **A 325**, 43-61, doi.org/10.1098/rsta.1988.0041

Johns, W. E., Shay, T. J., Bane, J. M., and D. R. Watts, 1995: Gulf Stream structure, transport, and recirculation near 68W. *J. Geophys. Res.*, **100**, 817–838, doi.org/10.1029/94jc02497

Johnson G. C., and M. J. McPhaden, 1999: Interior pycnocline flow from the subtropical to the equatorial Pacific Ocean. *J. Phys. Oceanogr.*, **29**, 3073-3089, doi.org/10.1175/1520-0485(1999)029<3073:ipffts>2.0.co;2

Kleidon, A., 2009: Non-equilibrium thermodynamics and maximum entropy production in the Earth system: applications and implications. *Naturwissenschaften*, **96**, 653–677, doi.org/10.1007/s00114-009-0509-x

Knauss, J. A., 1978: *Introduction to physical oceanography*. Prentice-Hall, 338 pp.

Krauss, W., and C. W. Böning, 1987: Lagrangian properties of eddy fields in the northern North Atlantic as deduced from satellite-tracked buoys. *J. Mar. Res.*, **45**, 259– 291, doi.org/10.1357/002224087788401142

LaCasce, J., and A. Bower, 2000: Relative dispersion in the subsurface North Atlantic. *J. Mar. Res.*, **58**, 863–894, doi.org/10.1357/002224000763485737

Leetmaa, A., Niiler, P., and H. Stommel, 1977: Does the Sverdrup relation account for the Middle Atlantic circulation? *J. Mar. Res*., **35**, 1-10.

Liu, T., Ou, H-W., Liu, X., and D. Chen, 2021: On the role of eddy mixing in the subtropical ocean circulation. Submitted to *J. Geophys. Res. Oceans.*

Lozier, M. S., 2010: Deconstructing the conveyer belt. *Science*, **328** (5985), 1507-1511, doi:10.1126/science.1189250

Lozier, M. S., Owens, W. B., and R. G. Curry, 1995: The climatology of the North Atlantic. *Prog. Oceanogr*., **36**(1), 1-44, doi.org/10.1016/0079-6611(95)00013-5

Luyten, J. R., Pedlosky, J., and H. Stommel, 1983: The ventilated thermocline. *J. Phys. Oceanogr.*, **13**, 292–309, doi.org/10.1175/1520-0485(1983)013<0292:tvt>2.0.co;2

Macdonald, A. M., 1998: The global ocean circulation: A hydrographic estimate and regional analysis. *Progr. Oceanogr.*, **41**(3), 281-382, doi.org/10.1016/s0079-6611(98)00020-2

Marshall, J., and G. Nurser, 1986: Steady, free circulation in a stratified, quasi-geostrophic ocean. *J. Phys. Oceanogr*., **16**,1799-1813, doi.org/10.1175/1520-0485(1986)016<1799:sfcias>2.0.co;2

Marshall, J., and G. Nurser, 1988: On the recirculation of the subtropical gyre. *Q. J. R. Meteorol. Soc*., **114**, 1517-1534, doi.org/10.1002/qj.49711448408

McCartney, M. S., 1982: The subtropical recirculation of mode waters. *J. Mar. Res*., **40** (Supp.), 427-464.

McDowell, S., Rhines, P. B., and T. Keffer, 1982: North Atlantic potential vorticity and its relation to the general circulation. *J. Phys. Oceanogr.*, **12**, 1417-1436, doi.org/10.1175/1520-0485(1982)012<1417:napvai>2.0.co;2

Munk, W. H., 1950: On the wind-driven circulation. *J. Meteor.*, **7**(2), 79-92, doi.org/10.1175/1520-0469(1950)007<0080:otwdoc>2.0.co;2

Nakamura, N., 1996: Two-dimensional mixing, edge formation, and permeability diagnosed in an area coordinate. *J. Atm. Sci*., **53**(11), 1524-1537, doi.org/10.1175/1520-0469(1996)053<1524:tdmefa>2.0.co;2

Nakamura, M., and T. Kagimoto, 2006: Potential vorticity and eddy potential enstrophy in the North Atlantic Ocean simulated by a global eddy-resolving model. *Dyn. Atm. Oceans*, **41**(1), 28-59, doi.org/10.1016/j.dynatmoce.2005.10.002

Niiler, P. P., 1986: The observational basis for large scale circulation of the oceans. In: *The General circulation of the ocean* (eds. H. Abarbenel and W. Young), Springer-Verlag, 1-54, doi.org/10.1007/978-1-4612-4636-7_1

Ollitrault, M., Gabillet, C., and A. Colin de Verdiere, 2005: Open ocean regimes of relative dispersion. *J. Fluid Mech*., **533**, 381–407, doi.org/10.1017/s0022112005004556

Ou, H. W., 2001: Possible bounds on the earth's surface temperature: From the perspective of a conceptual global-mean model. *J. Clim.*, **14**, 2976-2988, doi.org/10.1175/1520-0442(2001)014<2976:pbotes>2.0.co;2

992 Ou, H. W., 2006: Meridional thermal field of a coupled ocean-atmosphere system: a conceptual
993 model. *Tellus*, **58A**, 404-415, doi.org/10.1111/j.1600-0870.2006.00174.x

994 Ou, H. W., 2007: Hydrological cycle and ocean stratification in a coupled climate system: a the-
995 oretical study. *Tellus*, **59A**, 683-694, doi.org/10.3402/tellusa.v59i5.15157

996 Ou, H. W., 2013: Upper-bound general circulation of coupled ocean-atmosphere: Part 1. Atmos-
997 phere. *Dyn. Atm. Oceans*., **64**, 10-26, doi.org/10.1016/j.dynatmoce.2013.09.001

998 Ou, H. W., 2018: Thermohaline circulation: a missing equation and its climate change implica-
999 tions. *Clim. Dyn.*, **50**, 641–653, doi.org/10.1007/s00382-017-3632-y

1000 Ou, H. W., and W. de Ruijter, 1986: Separation of an inertial boundary current from curved
1001 coastline. *J. Phys. Oceanogr*., **16**, 280-289, doi.org/10.1175/1520-
1002 0485(1986)016<0280:soaibc>2.0.co;2

1003 Ozawa, H., Ohmura, A., Lorenz, R. D., and T. Pujol, 2003: The second law of thermodynamics
1004 and the global climate system: a review of the maximum entropy production principle. *Rev.*
1005 *Geophys.*, **41**(4), doi.org/10.1029/2002rg000113

1006 Parsons, A. T., 1969: A two layer model of Gulf Stream separation. *J. Fluid Mech.*, **39**, 511-528,
1007 doi.org/10.1017/s0022112069002308

1008 Pedlosky, J., 1983: Eastern boundary ventilation and the structure of the thermocline. *J. Phys.*
1009 *Oceanogr.*, **13**(11), 2038-2044, doi.org/10.1175/1520-0485(1983)013<2038:ebvats>2.0.co;2

1010 Pedlosky, J., 1991: The link between western boundary current and equatorial undercurrent. *J.*
1011 *Phys. Oceanogr.*, **21**, 1553-1558, doi.org/10.1175/1520-
1012 0485(1991)021<1553:tlbwbc>2.0.co;2

1013 Pierrehumbert, R. T., 1991: Large-scale horizontal mixing in planetary atmospheres. *Phys. Flu-*
1014 *ids*, **A3**(5), 1250-1260, doi.org/10.1063/1.858053

1015 Rahmstorf, S., Crucifix, M., Ganopolski, A., Goosse, H., Kamenkovich, I., Knutti, R., Lohmann,
1016 G., Marsh, R., Mysak, L. A., Wang, Z., and A. J. Weaver, 2005: Thermohaline circulation
1017 hysteresis: A model intercomparison. *Geophys. Res. Lett.*, **32**(23), L23605,
1018 doi:10.1029/2005GL023655

1019 Rhines, P. B., and W. R. Young, 1982: Homogenization of potential vorticity in planetary gyres.
1020 *J. Fluid Mech.*, **122**, 347-367, doi.org/10.1017/s0022112082002250

1021 Richardson, P. L., 1985: Average velocity and transport of the Gulf Stream near 55W. *J. Mar.*
1022 *Res.*, **43**, 83-111, doi.org/10.1357/002224085788437343

1023 Rossby, H. T., 1965: On thermal convection driven by non-uniform heating from below: an ex-
1024 perimental study. *Deep Sea Res.*, **12**, 9–16, doi.org/10.1016/0011-7471(65)91336-7

1025 Salmon, R., 1982: The shape of the main thermocline. *J. Phys. Oceanogr.*, **12**(12), 1458-1479,
1026 doi.org/10.1175/1520-0485(1982)012<1458:tsotmt>2.0.co;2

1027 Salmon, R., 1990: The thermocline as an “internal boundary layer.” *J. Mar. Res.*, **48**, 437-469,
1028 doi.org/10.1357/002224090784984650

Samelson, R. M., and G. K. Vallis, 1997: Large-scale circulation with small diapycnal diffusion: The two-thermocline limit. *J. Mar. Res.*, **55**(2), 223-275, doi.org/10.1357/0022240973224382

Sarmiento, J. L., 1983: A tritium box model of the North Atlantic thermocline. *J. Phys. Oceanogr.*, **13**, 1269-1274, doi.org/10.1175/1520-0485(1983)013<1269:atbmot>2.0.co;2

Schmitz, W. J., Thompson, J. D., and J. R. Luyten, 1992: The Sverdrup circulation for the Atlantic along 24 N. *J. Geophys. Res.* (*Oceans*), **97**(C5), 7251-7256, doi.org/10.1029/92jc00417

Stommel, H., 1948: The westward intensification of wind-driven ocean currents. *Trans. Am. Geophys. Union*, **29**, 2, 202-206, doi.org/10.1029/tr029i002p00202

Stommel, H., 1965: *The Gulf Stream: A Physical and Dynamical Description.* University of California Press, 197 pp.

Sverdrup, H. U., 1947: Wind-driven currents in a baroclinic ocean, with application to the equatorial currents of the eastern Pacific. *Proc. Natl. Acad. Sci. U.S.A.*, **33**, 318-326, doi.org/10.1073/pnas.33.11.318

Talley, L. D., Pickard, G. L., Emery, W. J., and J. H. Swift, 2011: *Introduction to Descriptive Physical Oceanography*. Academic Press, 560 pp.

Toole, J. M., Millare, R. C., Wang, Z., and S. Pu, 1990: Observations of the Pacific North Equatorial Current Bifurcation at the Philippine Coast. *J. Phys. Oceanogr.*, **20**, 307-318, doi.org/10.1175/1520-0485(1990)020<0307:ootpne>2.0.co;2

Tsuchiya, M., 1972: A subsurface north equatorial countercurrent in the eastern Pacific Ocean. *J. Geophys. Res.*, **77**, 5981-5986, doi.org/10.1029/jc077i030p05981

1050 Turiel, A., Nieves, V., García-Ladona, E., Font, J., Rio, M. H., and G. Larnicol, 2009: The mul-
1051 tifractal structure of satellite sea surface temperature maps can be used to obtain global maps
1052 of streamlines. *Ocean Science*, **5**(4), doi.org/10.5194/os-5-447-2009

1053 Veronis, G., 1973: Model of world ocean circulation. I. Wind-driven, two-layer. *J. Mar. Res*., **31**,
1054 228-288.

1055 Vreugdenhil, C. A., Gayen, B., and R. W. Griffiths, 2016: Mixing and dissipation in a geo-
1056 strophic buoyancy-driven circulation. *J. Geophys. Res. (Oceans)*, **121**, 6076–6091,
1057 doi.org/10.1002/2016jc011691

1058 Welander, P., 1968: Wind-driven circulation in one- and two-layer oceans of variable depth. *Tel-*
1059 *lus*, **20**, 1–15, doi.org/10.3402/tellusa.v20i1.9916

1060 Worthington, L. V., 1976: On the North Atlantic Circulation. *The Johns Hopkins Oceanographic*
1061 *Studies*, **6**, 110 pp.

1062 Wunsch, C., 1998: The work done by the wind on the oceanic general circulation. *J. Phys.*
1063 *Oceanogr*. **28**, 2332–2340, doi.org/10.1175/1520-0485(1998)028<2332:twdbtw>2.0.co;2

1064 Wunsch, C., 2011: The decadal mean ocean circulation and Sverdrup balance. *J. Mar. Res.*,
1065 **69**(2-3), 417-434, doi.org/10.1357/002224011798765303

1066 Wyrtki, K., and B. Kilonsky, 1984: Mean water and current structure during the Hawaii-to-Tahiti
1067 shuttle experiment. *J. Phys. Oceanogr*., **14**, 242-254, doi.org/10.1175/1520-
1068 0485(1984)014<0242:mwacsd>2.0.co;2

1069 Young, W. R., 1987: Baroclinic theories of the wind driven circulation. In *General Circulation*
1070 *of the Ocean*, H. D. I. Abarbanel and W. R Young, eds., Springer-Verlag, 291 pp.

1071

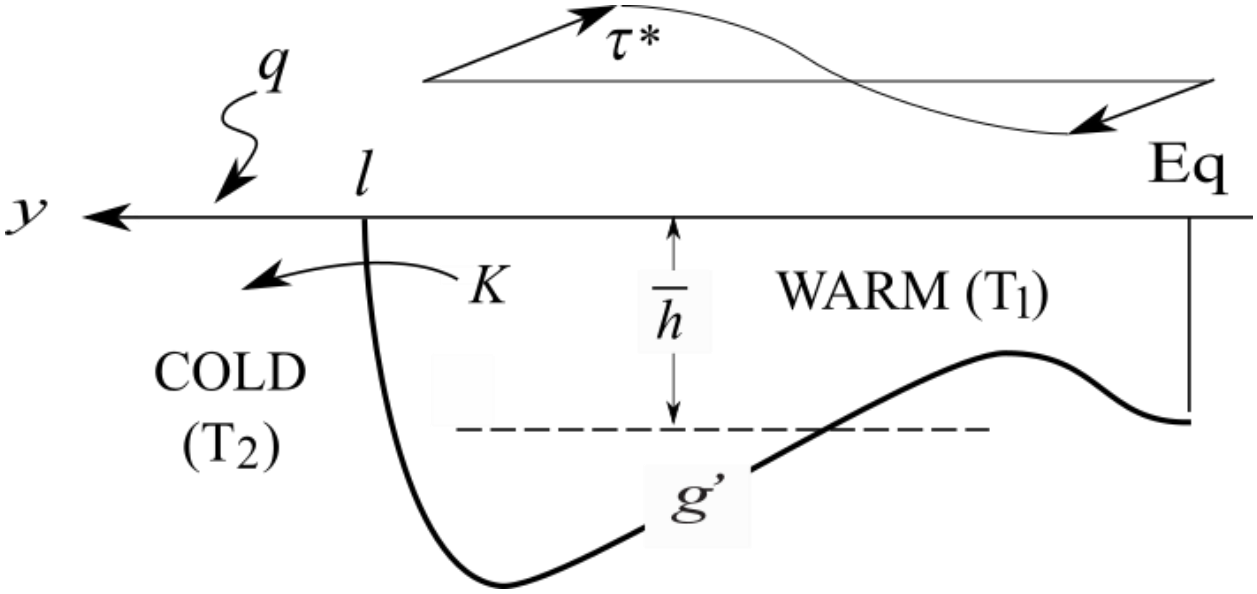


1073

1074 Fig. 1: The ocean configuration consisting of a moving warm layer separated from the motion-
1075 less cold water by an outcropped thermocline. The ocean is subjected to differential heating by
1076 the absorbed solar flux ($q$) and differential forcing by the wind stress ($\tau^*$). The prior constrains
1077 are the outcrop latitude ($l$), the mean depth ($\bar{h}$) and the reduced gravity ($g'$) of the thermocline as
1078 well as the MOC flux ($K$).

1079

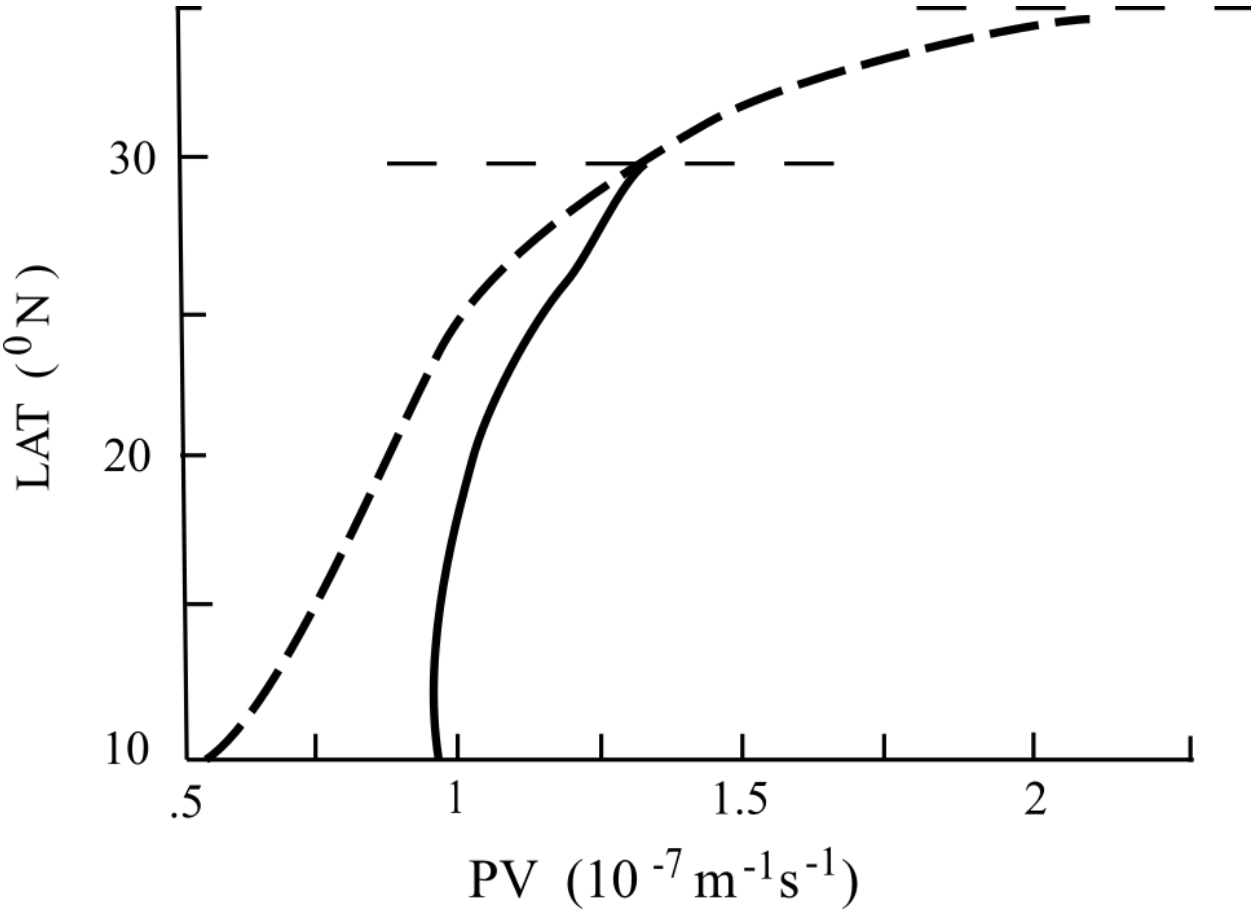


Fig. 2: Meridional profiles of the warm-layer PV from the coarse- (thick dashed) and fine-grained (thick solid) numerical calculations (taken from Liu et al. 2021), the dashed lines marking the outcrops. The eddy mixing has reduced the PV range to 20% of its laminar range.

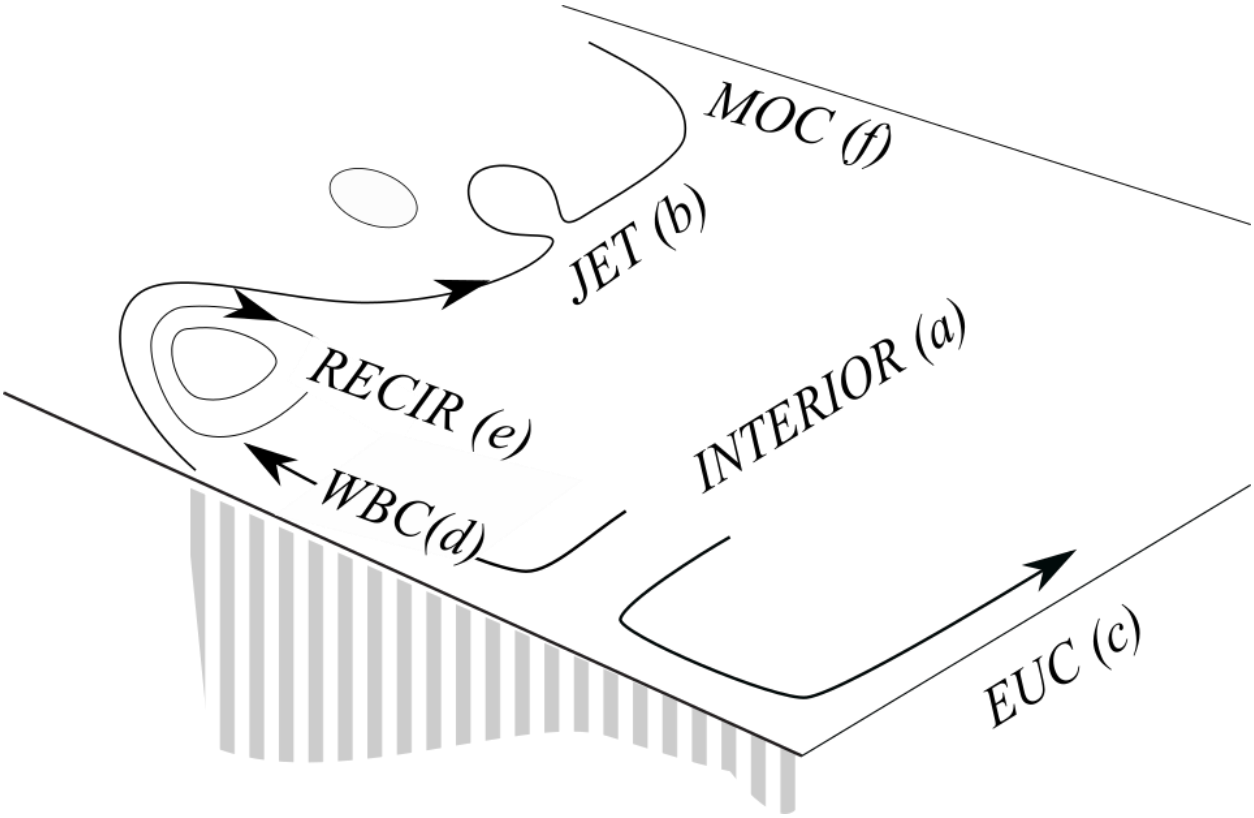


Fig. 3: Constituents of the model GOC, including the interior (a), the frontal jet (b), the EUC (c), the meridional boundary current (d), the recirculation (e) and the MOC (f), the letters marking the section headings.

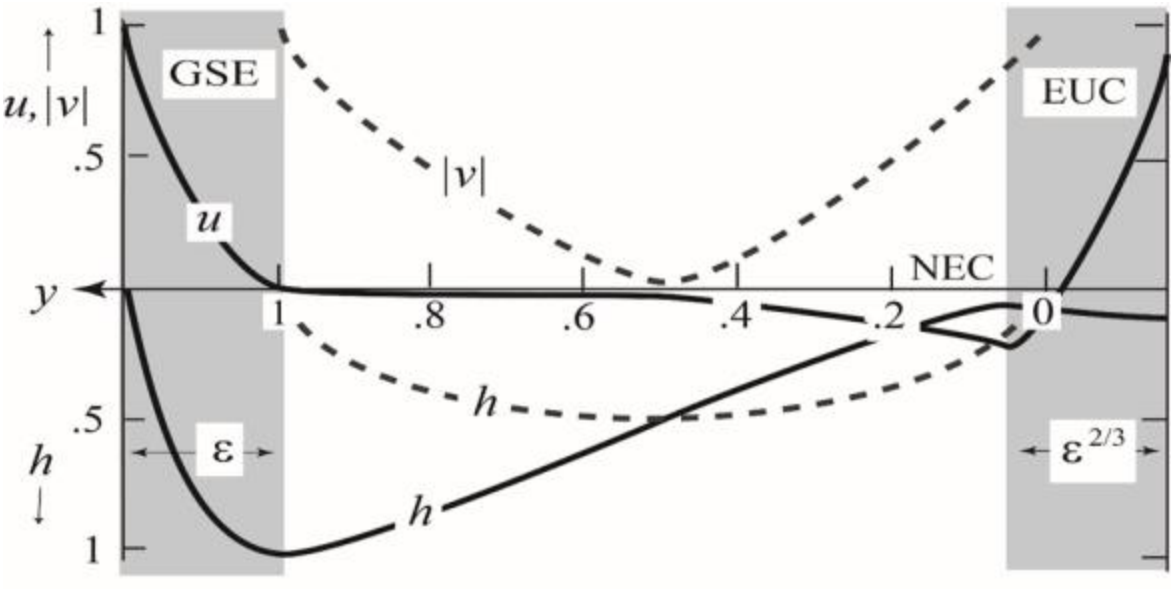


Fig. 4: The model solution plotted against the latitude. Solid lines are for the zonal interior ($h$, the thermocline depth and $u$, the eastward velocity) and dashed lines are for the meridional boundary layer ($h$, the thermocline depth and $|v|$, the meridional current speed). The boundary layers along the subtropical front and equator (shaded) have been magnified 21 and 5 times, respectively.

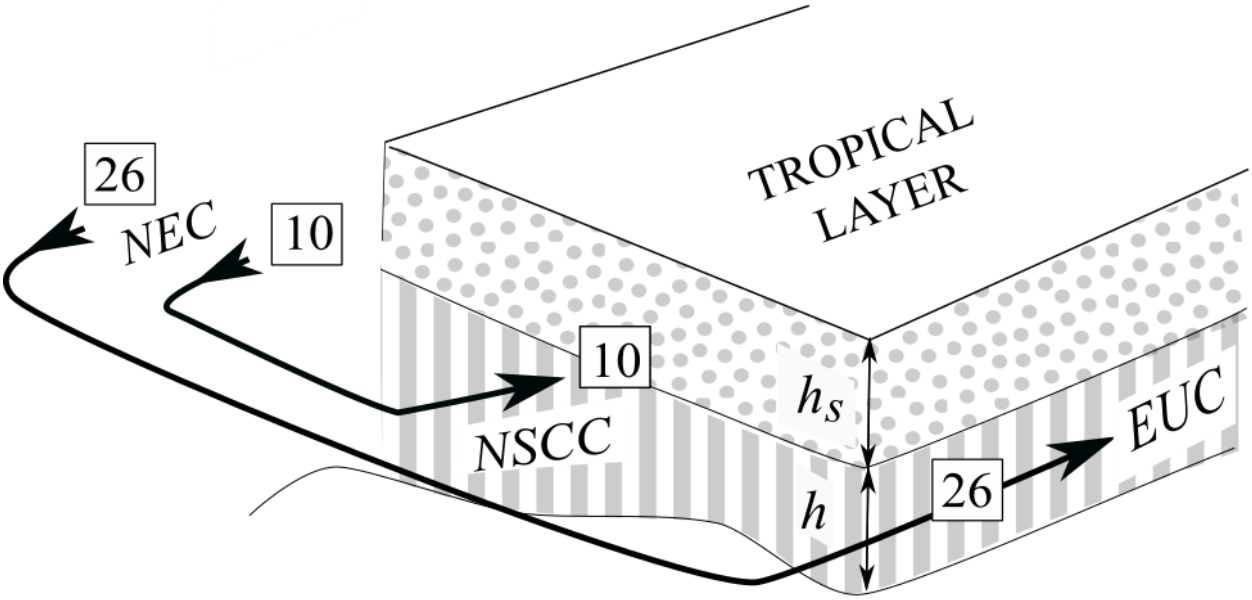


Fig. 5: A schematic of the EUC when overlain by a tropical layer (polka-dotted). The tropical layer depresses the main thermocline to weaken the EUC via the Bernoulli law. In addition, the tropical layer encroaches on the NEC to reduce the subtropical supply of the EUC, which is also syphoned by the NSCC, resulting in a much-reduced EUC transport.

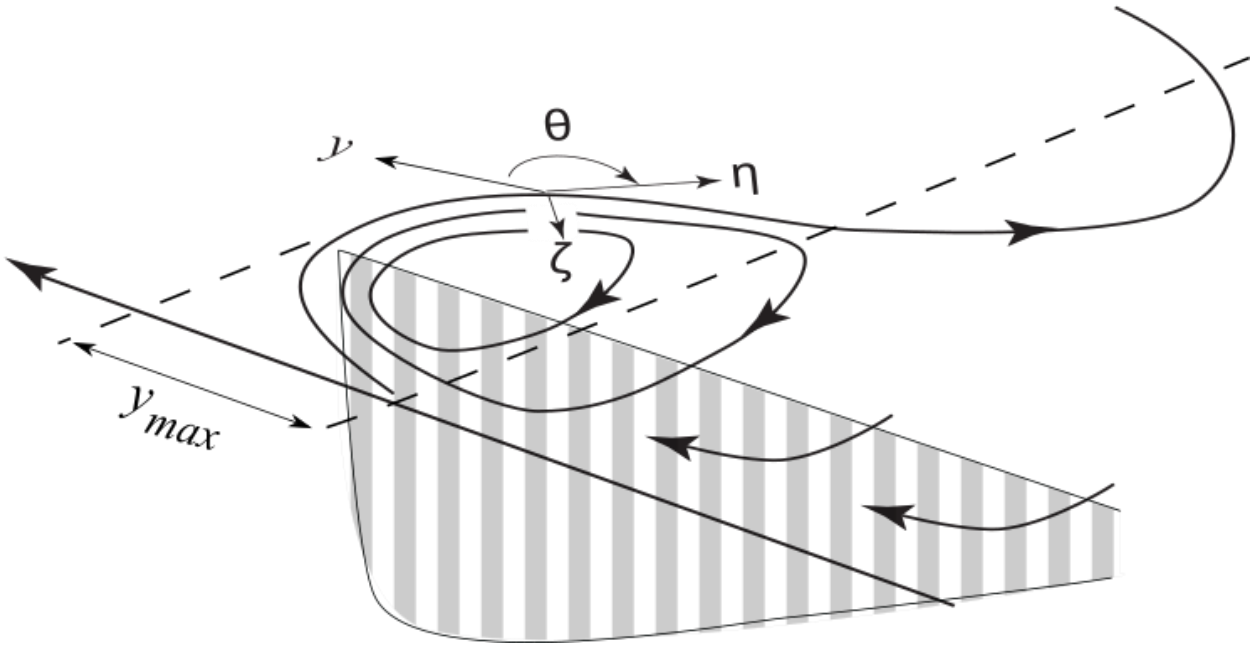


Fig. 6: A schematic of the recirculation. The separated jet traces out a beta-induced arc, which extends a distance $y_{max}$ beyond the separation point that is roughly the geometric mean of the deformation and earth's radii. Within the arc, the sloping thermocline due to the homogenized PV would drive a westward flow to augment the peak transport at the crest.